https://doi.org/10.5194/egusphere-2025-2107
Preprint. Discussion started: 15 May 2025

Impact of water uptake on fluorescence of atmospheric aerosols: Insights from Mie-Raman-Fluorescence lidar measurements

Igor Veselovskii[1], Qiaoyun Hu[2], Philippe Goloub[2], Thierry Podvin[2], Gaël Dubois[2], Alexey Kolgotin[1], Mikhail Korenskii[1]

[1]Prokhorov General Physics Institute of the Russian Academy of Sciences, Moscow, Russia
[2]Univ. Lille, CNRS, UMR 8518 - LOA - Laboratoire d'Optique Atmosphérique, F-59650 Lille, France

Correspondence to: Igor Veselovskii (igorv@pic.troitsk.ru)

Abstract. This study investigates the impact of water uptake by particles during hygroscopic growth on aerosol fluorescence properties, using multi-wavelength Mie-Raman-Fluorescence lidar measurements conducted at the ATOLL observatory (Laboratoire d'Optique Atmosphérique, University of Lille) between 2021 and 2024. During certain episodes we observed a systematic height-dependent decrease in the fluorescence backscattering coefficient within the well-mixed planetary boundary layer. This phenomenon begins at relatively low relative humidity (RH ~50%) simultaneously with decreasing the particle depolarization ratio. However, the rapid growth of aerosol backscattering coefficient at high RH is not mirrored by the same rate of fluorescence reduction. This distinct behaviour suggests a nonlinear relationship between water uptake and fluorescence suppression, likely indicating water-induced quenching effects that operate independently of bulk hygroscopic growth. Furthermore, we demonstrate the capability to retrieve particle volume and surface density from single-wavelength extinction coefficients during strong hygroscopic growth episodes, validated against full $3\beta+2\alpha$ lidar measurements. The values of the conversion factors for urban aerosol and smoke at 355 nm and 532 nm, together with associated uncertainties, are presented.

1 Introduction

Atmospheric aerosols are the subject of intense study due to their role in the planet's radiation balance and their potential impact on the environment. To characterize the vertical distribution of aerosol loading, multiwavelength Mie-Raman and high spectral resolution lidars are widely used (e.g., Burton et al., 2021; Floutsi et al., 2023, Haarig et al., 2025 and references therein). Studies conducted over the past two decades have demonstrated significant progress in retrieving particle microphysical properties such as volume density, effective radius, and complex refractive index from so-called $3\beta+2\alpha$ observations, which include three aerosol backscattering, β, and two extinction, α coefficients (Kolgotin et al., 2018, 2023, 2024; Chang et al., 2022; Zhou et al., 2024).

The $3\beta+2\alpha$ dataset is not always available; however, if the aerosol type is identified, the particle volume and surface densities can be estimated from the aerosol extinction coefficient at a single wavelength (λ), using corresponding extinction-to-volume and extinction-to-surface conversion factors, and . This approach was proposed by Mamouri and Ansmann (2017) and further developed by Ansmann et al. (2021), where optical depths and column-integrated volumes provided by the network of sun

https://doi.org/10.5194/egusphere-2025-2107
Preprint. Discussion started: 15 May 2025

photometers (AERONET) were used to determine conversion factors for pollution, smoke, and dust at various locations. Similarly, He et al. (2023) reported conversion factors for dust of different origins. However, the column-integrated values provided by the AERONET do not account for the possible presence of different aerosol types at different altitudes. In contrast, multiwavelength lidar measurements allow for the retrieval of vertical profiles of particle volume and surface density, enabling the calculation of conversion factors within specific height intervals that correspond to distinct aerosol types.

An important factor influencing the physical properties of aerosols is the relative humidity (RH). Many aerosol types, such as sulphates, organic carbon, and sea salt, increase in size at high RH, accompanied by a simultaneous decrease in their complex refractive index. Lidars, with their capability to assess particle properties under ambient conditions at RH levels close to saturation, offer unique opportunities for studying the particle hygroscopic growth. Lidar measurements are typically used to determine the dependence of the aerosol backscattering coefficient on RH within well-mixed layers (Feingold and Morley, 2003; Fernández et al., 2015; Granados-Muñoz et al., 2015; Haarig et al., 2017; Navas-Guzmán et al., 2019; Chen et al., 2019; Pérez-Ramírez et al., 2021; Sicard et al., 2022, Miri et al., 2024). The use of the aerosol extinction coefficients in hygroscopic growth studies is less common (Veselovskii et al., 2009; Dawson et al., 2020; Haarig et al., 2025), because β can be retrieved from lower altitudes and with greater accuracy compared to α. Multiwavelength lidar measurements further extend hygroscopic growth studies by enabling the analysis of particle volume, surface density, and the refractive index as a function of RH. This, in turn, allows for the evaluation of extinction-to-volume and extinction-to-surface conversion factors in the presence of hygroscopic growth.

The addition of a fluorescence channel to Mie-Raman lidar (Veselovskii et al., 2020) opens new opportunities for particle characterization. If hygroscopic growth has no impact on aerosol fluorescence properties, fluorescence may serve as a proxy for evaluation the volume of dry aerosol. However, the possibility of fluorescence being influenced by water uptake exists. In particular, fluorescence quenching of organic fluorophores in aqueous solutions has been reported by Dobretsov et al. (2014) and Maillard et al. (2021). Meanwhile, the extent to which such quenching occurs in atmospheric aerosols remains an open question (Gast et al., 2024; Reichardt et al., 2024). Fluorescence quenching is expected to depend on aerosol composition, highlighting the need to analyse a diverse set of measurement episodes.

The Mie-Raman-Fluorescence lidar has been operating at the ATOLL (ATmospheric Observation at LiLLe) instrumentation site at the Laboratoire d'Optique Atmosphérique, University of Lille, since 2020, accumulating a large volume of observations. In this paper, we focus on several episodes of hygroscopic growth within the planetary boundary layer (PBL), investigating potential evidence of fluorescence quenching by water uptake. Additionally, we analyze extinction-to-volume and extinction-to-surface conversion factors in the presence of hygroscopic growth. We begin with description of the lidar system and data analysis approach (Section 2). A numerical simulation of the relationship between particle volume and surface density on one hand and the extinction coefficient on the other, for different particle size distribution parameters, is presented in Section 3. In the first results section (Sections 4), we present case studies demonstrating that, in certain episodes, water uptake leads to fluorescence quenching. In Section 5, we analyse the conversion factors and in the presence of the particle hygroscopic growth. The paper concludes with a summary of our findings in the conclusion section.

https://doi.org/10.5194/egusphere-2025-2107
Preprint. Discussion started: 15 May 2025

2 Instrumentation and methodology

The multiwavelength Mie-Raman-Fluorescence lidar LILAS (LIlle Lidar AtmosphereS) operates using a tripled Nd:YAG laser with a 20 Hz repetition rate and a pulse energy of 90 mJ at 355 nm. Backscattered light is collected by a 400 mm aperture Newtonian telescope. Detailed information on the system parameters and data analysis methodology can be found in our previous publications (e.g. Veselovskii et al., 2020). Measurements were performed primarily in the vertical direction. In cases where measurements were taken at an angle, this information is provided in the figure captions. LILAS is designed to detect elastic and Raman backscattering, enabling the so called $3\beta+2\alpha+3\delta$ data configuration. This includes three particle backscattering (β_{355}, β_{532}, β_{1064}), two extinction (α_{355}, α_{532}) coefficients and three particle depolarization ratios (δ_{355}, δ_{532}, δ_{1064}). Additionally, the water vapor mixing ratio (WVMR) is derived from the water vapor Raman measurements. The lidar also profiles the laser-induced fluorescence of aerosol particles within a spectral interval centered at 466 nm with 44 nm bandwidth.

The fluorescence backscattering coefficient, β_F, and the fluorescence capacity, $G_F = \frac{\beta_F}{\beta_{532}}$, calculated from these measurements, facilitate aerosol classification, as described in Veselovskii et al. (2024).

The inversion of $3\beta+2\alpha$ lidar dataset enables the estimation of particle volume, V, surface, S, density and the RI. In our study, we used the inversion algorithm described by Veselovskii et al. (2002). The solution search was performed within the following parameter ranges:

- Particle radius: $0.05<r<10$ µm
- Real part of the refractive index: $1.33<m_R<1.65$
- Imaginary part of the refractive index: $0<m_I<0.02$

The retrieval uncertainty for particle volume and surface density is estimated to be below 15%, while for the real part of the refractive index it is ±0.05. The uncertainty for the imaginary part is higher, reaching up to 50%. Therefore, in the analysis of the presented measurements, only the real part of the refractive index is considered. Retrieved values of V and S enable the calculation of extinction-to-volume and extinction-to surface conversion factors, defined as $C^V_{\alpha,\lambda} = \frac{V}{\alpha_\lambda}$ and $C^S_{\alpha,\lambda} = \frac{S}{\alpha_\lambda}$ respectively. These factors allow for the estimation of V and S from a single extinction coefficient at wavelength λ, when the aerosol type is known. Corresponding conversion factors can also be defined for backscattering coefficients.

To assess the effect of water uptake on fluorescence, we selected episodes where the PBL was well mixed, ensuring that aerosol composition and particle number density remained unchanged with height. A well-mixed layer was identified based on stable WVMR and potential temperature. The potential temperature was available from radiosonde measurements at Herstmonceux (UK) and Beauvechain (Belgium) stations, located 160 km and 80 km away from the observation site, respectively. The height profiles of relative humidity were calculated using lidar-derived WVMR and temperature profiles from the radiosonde data.

https://doi.org/10.5194/egusphere-2025-2107
Preprint. Discussion started: 15 May 2025

Within the well-mixed PBL, relative humidity increases with height, leading to an increase in the aerosol extinction and backscattering coefficients. However, these coefficients respond differently to changes in RH. Water uptake reduces the particle refractive index, but the extinction coefficient is less sensitive to the refractive index changes than backscattering. As a result, during hygroscopic growth α increases more rapidly with RH than β, causing the extinction-to-backscattering ratio (lidar ratio) to rise. Dependence of backscattering on RH can follow either monotonic or a deliquescent pattern. In the deliquescent case, backscattering starts to increase fast when the deliquescence RH is reached (Carrico et al., 2003). For relative humidity exceeding the deliquescence value, the dependence of particle parameters, such as β, m_R, r, and V, on RH can be modeled on relative to their values at a some reference height, z_{ref}. In particular, for the backscattering coefficient the simplified Hänel parameterization is commonly used (Hänel, 1976; Sheridan et al., 2002; Sicard et al., 2022):

$$\frac{\beta}{\beta_{ref}} = \left(\frac{1-RH}{1-RH_{ref}}\right)^{-\gamma_\beta} \quad (1)$$

The subscript “ref” denotes the values of the parameters at the reference height z_{ref}; γ_β is the backscattering hygroscopic growth coefficient. The changes in particle radius, r, and m_R with relative humidity can be modeled in a similar manner (Hänel, 1976; Randriamiarisoa et al., 2006; Raut and Chazette, 2008):

$$\frac{r}{r_{ref}} = \left(\frac{1-RH}{1-RH_{ref}}\right)^{-\varepsilon} \quad (2)$$

$$m_R = m_R^{H2O} + (m_{R,ref} - m_R^{H2O})\left(\frac{r}{r_{ref}}\right)^{-3} = m_R^{H2O} + (m_{R,ref} - m_R^{H2O})\left(\frac{1-RH}{1-RH_{ref}}\right)^{3\varepsilon} \quad (3)$$

where m_R^{H2O} is the real part of the refractive index of water; ε is the size growth coefficient, which depends on aerosol chemical composition. The real part of the refractive index, modeled using Eq.3, will hereafter be denoted as m_R^{mod}. Parameterization (2) can also be applied to model the particle volume relative to its value, V_{ref}, at the reference height:

$$V^{mod} = V_{ref}\left(\frac{1-RH}{1-RH_{ref}}\right)^{-3\varepsilon} \quad (4)$$

When the vertical profile of particle volume density retrieved from $3\beta+2\alpha$ observations, V^{3+2}, is available, the ratio $\left(\frac{r}{r_{ref}}\right)^{-3}$ in Eq.3 can be replaced by $\frac{V_{ref}^{3+2}}{V^{3+2}}$ allowing to calculate the m_R as follows:

https://doi.org/10.5194/egusphere-2025-2107
Preprint. Discussion started: 15 May 2025

$$m_R = m_R^{H2O} + (m_{R,ref} - m_R^{H2O})\frac{V_{ref}^{3+2}}{V^{3+2}} \quad (5)$$

The real part of the refractive index, calculated using Eq.4, will be denoted as m_R^V. Recall that Eqs. (3)-(5) are applicable only within a well-mixed layer. The m_R at reference height, $m_{R,ref}$, in Eqs. (3) and (5) can be selected from the values retrieved from *3β+2α* observations, which will be denoted as m_R^{3+2}.

If water uptake does not alter the chemical composition and does not cause fluorescence quenching, the fluorescence signal should be proportional to the volume of dry particles. Thus, the variation of the fluorescence backscattering coefficient, β_F, relatively to its value at the reference height, $\beta_{F,ref}$, allows for modelling m_R within the layers, where particle number density varies with height, assuming the particle type remains unchanged. For this purpose, the expression $\frac{V_{ref}^{3+2}}{V^{3+2}}$ in Eq.5 should be replaced with $\frac{V_{ref}^{3+2}}{V^{3+2}}\frac{\beta_F}{\beta_{F,ref}}$:

$$m_R = m_R^{H2O} + (m_{R,ref} - m_R^{H2O})\frac{V_{ref}^{3+2}}{V^{3+2}}\frac{\beta_F}{\beta_{F,ref}} \quad (6)$$

The real part of the refractive index, modeled with Eq.6, will be denoted as m_R^F.

Our approach to identifying the potential effect of water uptake on fluorescence is based on analyzing episodes of strong hygroscopic growth within the well-mixed PBL. A decrease in fluorescence backscattering with height may indicate the occurrence of fluorescence quenching. Additionally, we compare the profiles of the real part of the refractive index, retrieved from *3β+2α* observations (m_R^{3+2}), with the modeled values m_R^F. A significant deviation of m_R^F from m_R^{3+2} at high RH could also suggest the presence of fluorescence quenching.

.

3 Numerical simulation of the particle volume and surface density as a function of the extinction coefficient

We begin with a numerical simulation to explore the relationship between particle volume and surface density, on one hand, and the extinction coefficient, on the other, for different particle sizes and refractive indices. In this simulation, we consider a set of lognormal particle size distributions (PSDs) for the number density *n(r)*:

$$\frac{dn(r)}{d\ln r} = \frac{N}{(2\pi)^{1/2}\ln\sigma}\exp\left[-\frac{(\ln r - \ln r_0)^2}{2(\ln\sigma)^2}\right] \quad (7)$$

https://doi.org/10.5194/egusphere-2025-2107
Preprint. Discussion started: 15 May 2025

where N is the total particle number (N=1 in all computations). The mode radius, r_0, and $\ln\sigma$ varied within the [0.015-6.3] µm and the [0.43-0.936] intervals respectively. The particle extinction coefficient at 532 nm, α_{532}, was computed for spherical particles with the real and the imaginary part of the refractive index within the ranges [1.3-1.7] and [0.00-0.03] respectively. In total, more than 10^5 extinction coefficients were calculated, using the look-up-tables (Kolgotin et al., 2023).

The results of the computations are summarized in Fig.1, which shows particle volume and surface density as a function of the extinction coefficient at 532 nm. To provide insight into the particle sizes corresponding to different α_{532}, the upper axis presents approximate values of the effective radius, r_{eff}. The ratio $\frac{V}{\alpha_{532}}$ in Fig.1a exhibits a tendency to increase with particle size, and for a given value of α_{532} this ratio varies significantly, spanning up to an order of magnitude. However, for specific aerosol types, the dependence $V(\alpha_{532})$, which characterizes particle hygroscopic growth, can be reasonably approximated by a linear fit.

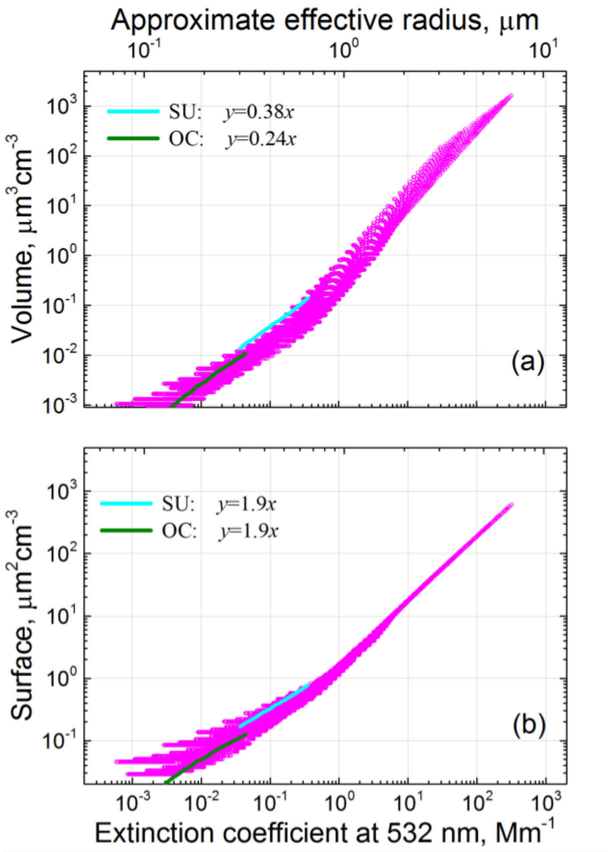

Figure 1: Modeled particle (a) volume and (b) surface density as functions of the extinction coefficient at 532 nm. The particle parameters used in the computations are described in the text.

https://doi.org/10.5194/egusphere-2025-2107
Preprint. Discussion started: 15 May 2025

Fig.1 presents also the data points, corresponding to the hygroscopic growth of two model aerosol types: sulfates (SU) and organic carbon (OC). The particle parameters used in the computations, such as mode radius and the refractive index, are based on values from MERRA-2 model (Chin et al., 2002; Colarco et al., 2010) and are summarized in Table A1 for different relative humidities. The $ln\sigma$ in Eq.7 was set to 0.79 for organic carbon (OC) and 0.71 for sulfate (SU) independent of RH. For the applied model, the volumes of SU and OC particles during hygroscopic growth can be linearly approximated as V=0.38α_{532}, V=0.24α_{532} respectively, where volume is expressed in μm^{3}cm^{-3} and the extinction coefficient in Mm^{-1}. These modeling results suggest that, even in the presence of hygroscopic growth, aerosol-type-specific conversion factors can still enable estimation of particle volume from the extinction coefficient. The variation of $\frac{S}{\alpha_{532}}$ in Fig.1b is significantly smaller compared to the $\frac{V}{\alpha_{532}}$ in Fig.1a, and it decreases with particle size, allowing for a more accurate estimation of surface density.

4 Results of observation

4.1 March 25, 2022. Hygroscopic growth within the well-mixed PBL

We begin with the episode on March 25, 2022, when the fluorescence backscattering remained relatively stable within the PBL. As shown in Fig. 2, variations in WVMR within the 650–1750 m height range remain below 0.3 g kg^{-1}, while potential temperature deviations are within 1.5 K. These conditions indicate that the PBL is well mixed. The relative humidity increases with height from 35% to 75%, resulting in a 1.5-fold increase in β_{532}. Using parameterization (1), the backscattering growth coefficient, γ_β, is estimated to be about 0.45. During hygroscopic growth, the particle depolarization ratio, δ_{532}, decreases with height from 10% to 5%, while the extinction Ångström exponent (*EAE*), calculated from α_{355} and α_{532}, decreases from 1.4 to 0.9. The fluorescence capacity at 650 m is G_F=0.65×10^{-4} and according to the classification scheme in Veselovskii et al. (2024), this corresponds to urban aerosol. This classification is further supported by HYSPLIT Backward Trajectory Analysis, which indicates that the air masses at this altitude originated from Germany.

The profile of particle volume, retrieved from $3\beta+2\alpha$ observations, V^{3+2}, is presented in Fig.2c, along with the corresponding conversion factors $C^V_{\alpha,532}$ and $C^V_{\beta,532}$ shown in Fig.3a. The conversion factor $C^V_{\alpha,532}$ remains relatively stable during hygroscopic growth, with a deviation from the mean value of about 10%. As shown in Fig.2c, the volume, V^α, calculated from α_{532} as $V^\alpha = C^V_{\alpha,532} \times \alpha_{532}$, aligns well with V^{3+2}, when using a mean conversion factor C^α_V =0.15 μm^{3}cm^{-3}Mm. On the other hand, the conversion factor $C^V_{\beta,532}$ exhibits higher variability (up to 20%), as it is sensitive to changes of the refractive index.

Fig.2c also displays the profile of V^{mod}, modeled using Eq.4 with z_{ref}=690 m. The size growth coefficient, ε, reported by Randriamiarisoa et al. (2006) for urban aerosol in Paris was 0.26. However, for our observations a better fit with V^{3+2} was achieved when using ε=0.33.

https://doi.org/10.5194/egusphere-2025-2107
Preprint. Discussion started: 15 May 2025

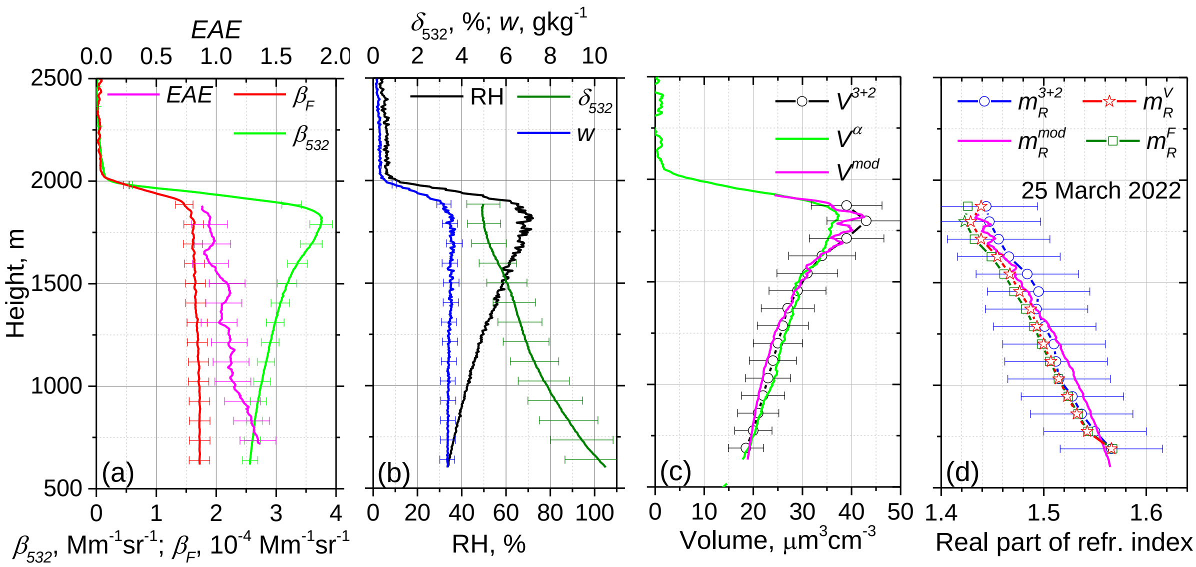

Figure 2: Vertical profiles of the particle parameters on 25 March 2022 for period 19:10-21:30 UTC. (a) The backscattering coefficient, β_{532}, the fluorescence backscattering coefficient, β_F, and the Ångström exponent, EAE. (b) The particle depolarization ratio, δ_{532}, the water vapor mixing ratio, *w*, and the relative humidity, RH. (c) The particle volume, V^{3+2}, retrieved from $3\beta+2\alpha$ observations; the volume, V^{α}, calculated from extinction coefficient α_{532} and the volume V^{mod} modeled with Eq.4 using ε=0.33. (d) The real part of the refractive index, m_R^{3+2}, retrieved from $3\beta+2\alpha$ observations, along with the values m_R^{mod}, modeled with Eq.3 and the values of m_R^V and m_R^F calculated from Eqs. (5) and (6) respectively. Measurements were performed at 48 deg to horizon.

The real part of the refractive index, m_R^{3+2}, retrieved from $3\beta+2\alpha$ observations, in Fig.2d decreases with height from 1.57 to 1.44 and it agrees with Hänel parametrization, m_R^{mod}, calculated with Eq.3 using $m_{R,ref}$ =1.57 at z_{ref}=700 m. The profiles of m_R^V and m_R^F calculated with Eqs. (5) and (6) respectively, align with m_R^{3+2} within the uncertainty of retrieval. Thus, for this specific case, we see no evidence for the fluorescence quenching by the water uptake.

The $3\beta+2\alpha$ observations enable the estimation of key characteristics of the particle size distribution, at least, for fine-mode particles. As the maximum available laser wavelength is 1064 nm, the retrievals exhibit decreasing sensitivity to particles with radii larger than approximately 2 µm (Veselovskii et al., 2009). The evolution of $\frac{dV}{d\ln r}$ with height is shown in Fig.3b. At 700 m, the fine mode, with a maximum at r=0.15 µm, is dominant. By 1700 m the maximum of the PSD shifts to approximately r=0.25 µm due to hygroscopic growth. A small secondary maximum at r=1.0 µm also appears; however we cannot conclusively determine whether it is a real feature or merely an artifact of the retrieval process. From this figure, we can conclude that, for the episode considered, the hygroscopic growth primarily affects fine-mode particles.

https://doi.org/10.5194/egusphere-2025-2107
Preprint. Discussion started: 15 May 2025

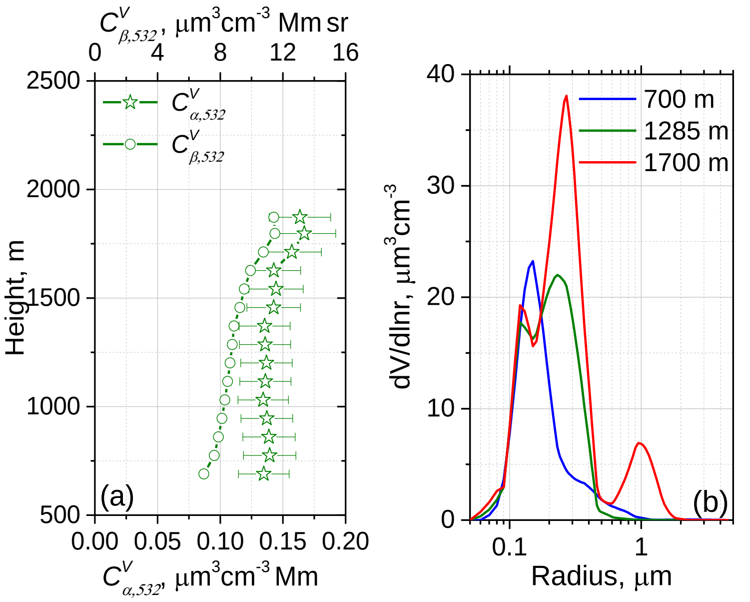

Figure 3: (a) Vertical profiles of extinction-to-volume, $C^V_{\alpha,532}$, and backscattering-to-volume, $C^V_{\beta,532}$, conversion factors on March 25, 2022. (b) The particle size distribution $\frac{dV}{d\ln r}$ at heights 700, 1285 and 1700 m.

4.2 August 30-31, 2022. Hygroscopic growth within not well-mixed layer

On August 30–31, 2022, an episode of pronounced hygroscopic growth was observed. The vertical profiles of the particle parameters, similar to those shown in Fig. 2, are presented in Fig.4 for August 30, 2022. Complete geometrical overlap of the laser beam and the telescope's field of view occurred around 1200 m; therefore, the extinction profiles and inversion results are available only above this height. The WVMR shows significant height variations within the 1200-2500 m range, indicating that this layer is not well-mixed. The HYSPLIT Backward Trajectory Analysis indicates that the air masses at the 1000 m height level originated from the north of Germany, while at higher altitudes they arrived from the Atlantic region and may have transported maritime particles. The relative humidity increases steadily with height and peaking at approximately 80% near 1750 m. Above this level, RH gradually decreases. Within the 1000–2500 m range, aerosol particles undergo hygroscopic growth, and the peak in the backscattering coefficient, β_{532}, is consistent with the RH maximum at this level. which peaks at 1750 m. In contrast, both the Ångström exponent and the linear depolarization ratio exhibit distinct minima at 1750 m.

The particle volume was retrieved from $3\beta+2\alpha$ observations, allowing calculation of the conversion factors $C^V_{\alpha,532}$ and $C^V_{\beta,532}$, as shown in Fig.5a. The deviation of $C^V_{\alpha,532}$ from its mean value is less than 15%, while for $C^V_{\beta,532}$ the deviation is larger, about 30%. The profile of the particle volume V^{α} calculated using the mean conversion factor $C^V_{\alpha,532}$=0.23 µm³cm⁻³Mm, aligns well with V^{3+2} in Fig.4c.

https://doi.org/10.5194/egusphere-2025-2107
Preprint. Discussion started: 15 May 2025

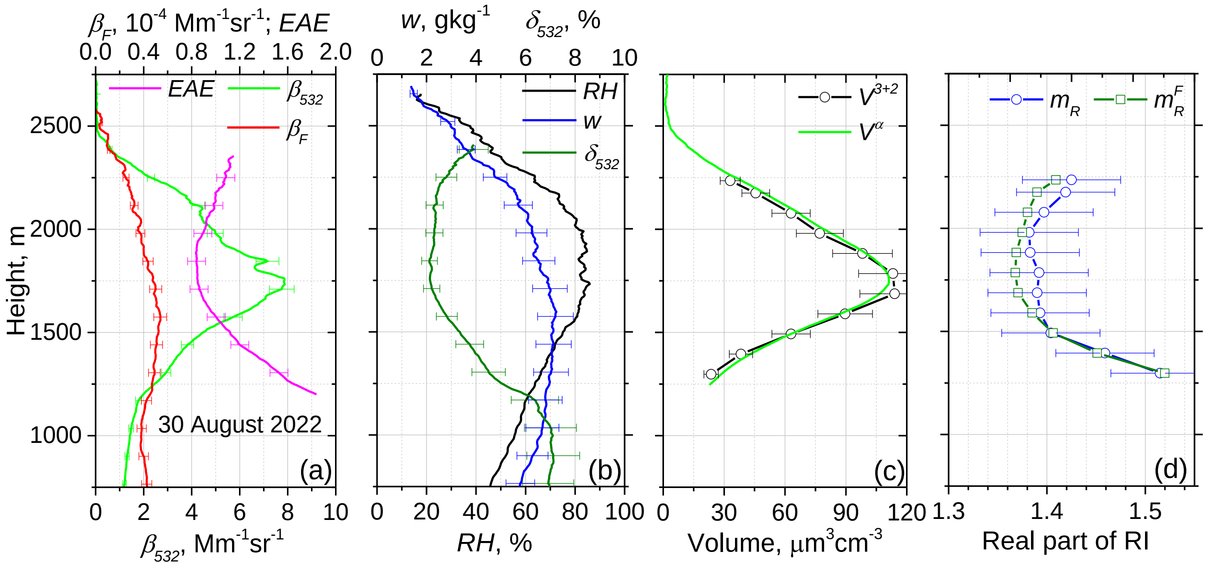

Figure 4: Similar to Fig.2 but for the measurements on 30 August 2022 during period 19:30-20:30 UTC.

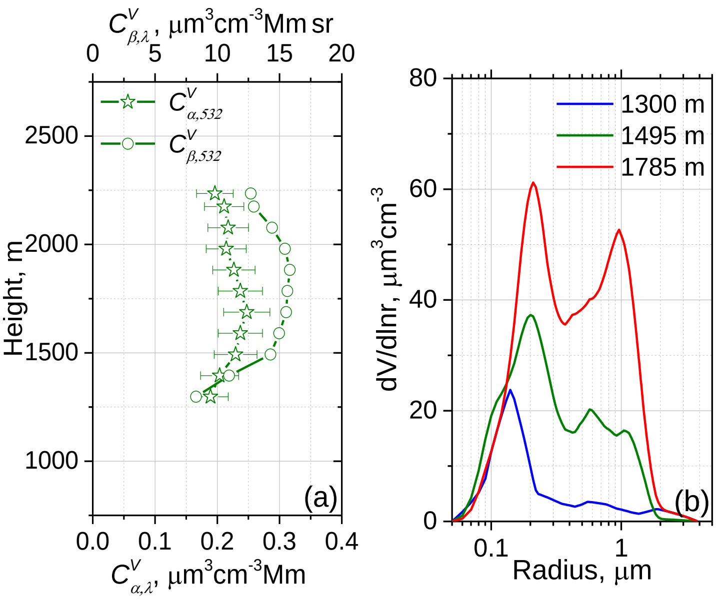

Figure 5: Similar to Fig.3 but for the measurements on August 30, 2022 during period 19:30-20:30 UTC.

The retrieved m_R^{3+2} decreases with height from 1.52 to 1.39 within the 1250-1750 m range, and then begins to increase above this level. The Hänel parameterization (3) and the calculation of m_R^V using Eq.5 are not applicable here, as the layer is not

https://doi.org/10.5194/egusphere-2025-2107
Preprint. Discussion started: 15 May 2025

well-mixed. However, the fluorescence backscattering allows the calculation of m_R^F via Eq.6. The reference value $m_{R,ref}$ is set to 1.52 at 1300 m and, as shown in Fig.4d, m_R^F, agrees with m_R^{3+2} within the uncertainty of retrieval. Thus, in this episode, once again, water uptake does not exhibit a significant effect on the fluorescence signal.

The modification of the PSD during hygroscopic growth is shown in Fig.5b. The maximum of the fine mode, within the 1300-1800 m range, shifts with height from r= 0.14 µm to r= 0.2 µm. Simultaneously, the second mode, centered near 1.0 µm, increases with height. This suggests that the aerosol mixture likely contains coarse hygroscopic particles, which could have a maritime origin.

4.3 Possibility of fluorescence quenching by the water uptake

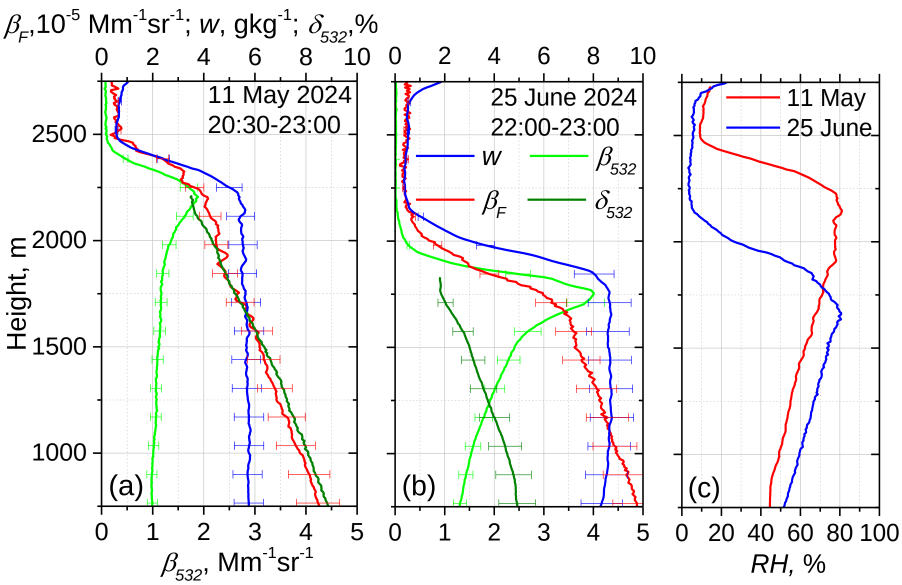

Figure 6: Vertical profiles of aerosol and fluorescence backscattering coefficients, β_{532} and β_F, along with water vapor mixing ratio, w, and the particle depolarization ratio, δ_{532}, measured on (a) 11 May 2024, (b) 25 June 2024. (c) The relative humidity for the episodes considered.

The assumption that fluorescence backscattering is independent of water uptake is crucial when using the fluorescence technique to study aerosol hygroscopic growth (Miri et al., 2024). However, in some episodes we observed a decrease in β_F with height within the well-mixed PBL, which may indicate possible fluorescence quenching. Two such episodes, on May 11 and June 25, 2024, are shown in Fig.6. In both cases, the PBL is well mixed, with variations in WVMR remaining below 0.2 gcm^{-3}. The air masses within the 500-2500 m range for both episodes originated from Germany. The fluorescence capacities at 750 m for these cases are 0.86×10^{-4} and 0.75×10^{-4} respectively, which is higher than for previous episodes. Due to hygroscopic growth, the backscattering β_{532} increases with height by a factor 1.8 on May 11, and by a factor 3 on June 25. The corresponding backscattering growth coefficients, γ_β, are estimated as 0.35 and 1.0 respectively. In contrast to results in Fig.2a,

https://doi.org/10.5194/egusphere-2025-2107
Preprint. Discussion started: 15 May 2025

the fluorescence backscattering, β_F, decreases with height along with δ_{532}. This decrease begins at relatively low RH, and the rapid increase in β_{532} at high RH is not accompanied by a similarly fast decrease in β_F.

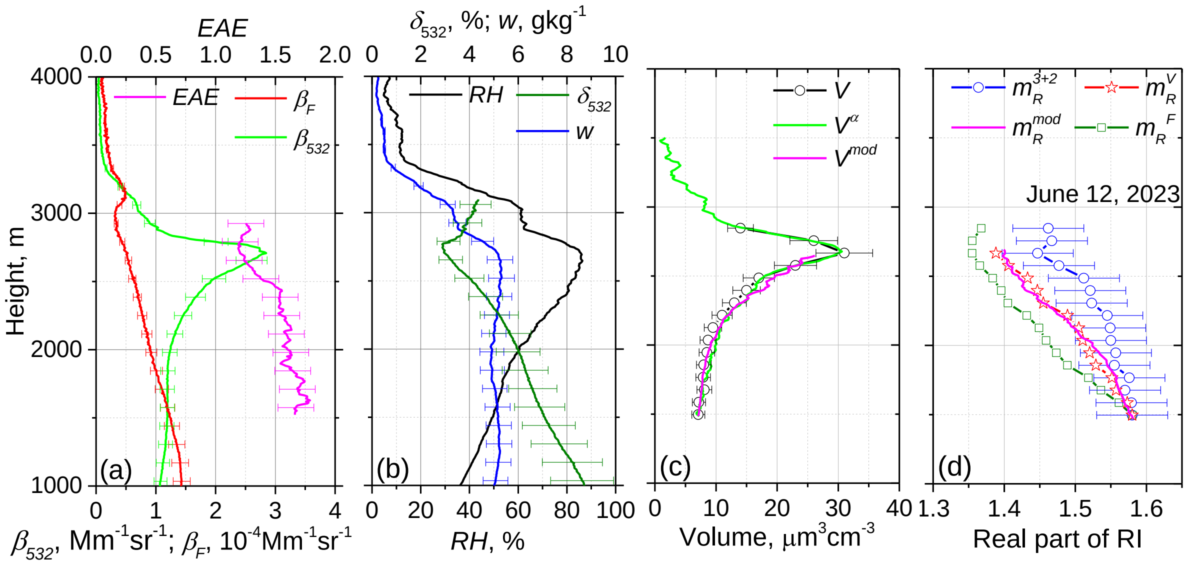

Figure 7: Similar to Fig.2 but for the measurements on June 12, 2023 for the period 21:00-22:20.

Among several episodes demonstrating the fluorescence quenching, one of the most representative occurred on June 12, 2023. Corresponding profiles of particles parameters are shown in Fig.7. Variations in WVMR and potential temperature within the 1000-1750 m range are small (below ±0.2 gkg^{-1} and ±2K respectively) indicating that the PBL is well-mixed. The HYSPLIT Backward Trajectory Analysis indicates that the air masses within the 1000-3000 m height range originated from Eastern Europe. The fluorescence capacity at 1000 m is quite high (1.32×10^{-4}), suggesting the presence of organic particles.

Within the 1000-2700 m altitude range the backscattering coefficient, β_{532}, shows a consistent positive response to RH, reaching its maximum value at 2700 m where RH peaks. The backscattering growth coefficient, γ_β, is determined to be approximately 0.7. Simultaneously, the observed increase in RH correlates with reduced fluorescence backscattering, suggesting potential fluorescence quenching effects. The aerosol volume, V^α, derived from α_{532} measurements shows good agreement with V^{3+2}, when applying a mean conversion factor C_V^α=0.15 µm^{3}cm^{-3}Mm. The modeled volume profile, V^{mod}, calculated using Eq.4 and ε=0.33, similarly matches V^{3+2} within the layer, where aerosols are presumed to be well-mixed.

The real part of the refractive index, m_R^{3+2}, retrieved from 3β+2α observations, decreases from 1.58 to 1.45, within the 1500-2700 m altitude range. However, this observed decrease occurs at a lower rate compared to both m_R^{mod} and m_R^V modeled values. Furthermore, the values, m_R^F, derived using the fluorescence signal in Eq.6, The values of m_R^F, calculated with use

https://doi.org/10.5194/egusphere-2025-2107
Preprint. Discussion started: 15 May 2025

270 of the fluorescence signal in Eq.6, are systematically lower than both m_R^{mod} and m_R^V, providing additional evidence for potential fluorescence quenching effects. Fig.8 shows the PSDs for three episodes, discussed in this section. As the particles undergo hygroscopic growth, the fine mode shifts toward larger radii; however, the second mode at r=1 μm, observed in Fig.5b, is absent. This suggests that only fine particles are undergoing hygroscopic growth.

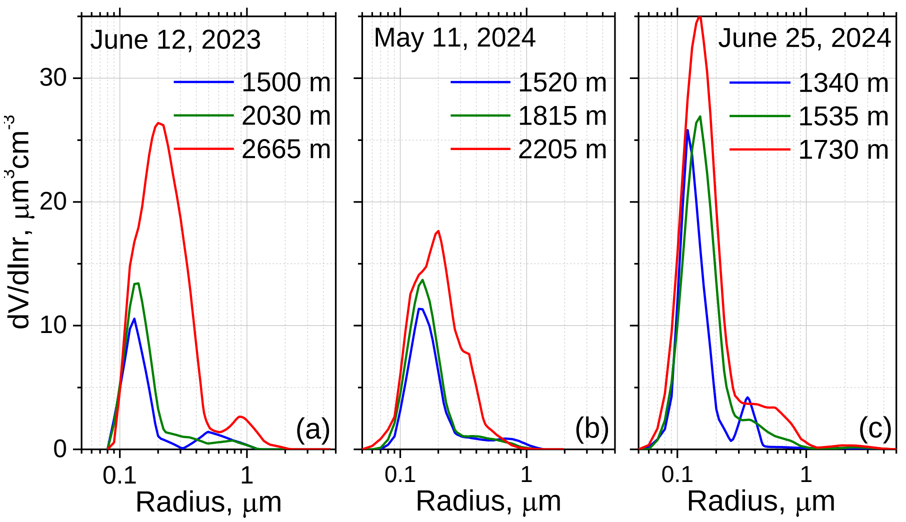

275 **Figure 8: The particle size distribution $\frac{dV}{d\ln r}$ at different heights for three case studies showing evidence of fluorescence quenching during hygroscopic growth: (a) June 12, 2023; (b) May 11, 2024; (c) June 25, 2024.**

To quantify fluorescence quenching effects we computed the relative reduction in fluorescence backscattering using:

$$\Delta\beta_F = \frac{\beta_{F,ref} - \beta_F}{\beta_{F,ref}} \tag{8}$$

280 Fig.9a displays the normalized β_{532} and fluorescence reduction $\Delta\beta_F$ as a function of RH for three observational periods: March 25, 2022, June 12, 2023 and May 11, 2024. For consistent comparison, β_{532} values were normalized to the backscattering coefficient at RH_{ref}=50% and $\Delta\beta_F$ were calculated for the same RH_{ref}. These case were selected based on two criteria: consistent β_{532}(RH) growth patterns across all events and distinctive variations in $\Delta\beta_F$ behavior between cases. As previously noted, the March 25, 2022 case showed no significant RH-dependent increase in $\Delta\beta_F$. In contrast, during the other two episodes (June 285 12, 2023 and May 11, 2024), $\Delta\beta_F$ exhibited a steady increase from baseline conditions reaching a maximum reduction of ~50% at RH = 85%. However, the rapid growth of β_{532} at high RH is not mirrored by the same rate of increase in $\Delta\beta_F$. This decoupling between hygroscopic backscattering growth and fluorescence suppression suggests that water uptake affects aerosol fluorescence through mechanisms beyond simple dilution effects.

https://doi.org/10.5194/egusphere-2025-2107
Preprint. Discussion started: 15 May 2025

To further investigate water uptake effect on fluorescence, Fig.9b presents the relationship between fluorescence reduction $\Delta\beta_F$ and particle volume V^{α}, calculated from α_{532}, for the same three case studies as in Fig.9a. On June 12, 2023 and May 11, 2024 $\Delta\beta_F$ demonstrates sharp increase within ~5–12 $\mu m^3 cm^{-3}$ volume range and a subsequent plateau at higher volumes. These observations reveal two key findings: quenching starts at relatively low RH (before maximum hygroscopic growth) and the $\Delta\beta_F$–volume relationship is nonlinear, disproving simple proportional dependence on water uptake. While aerosol-type dependence is evident, the specific particle composition driving this quenching behaviour cannot yet be definitively identified from these measurements.

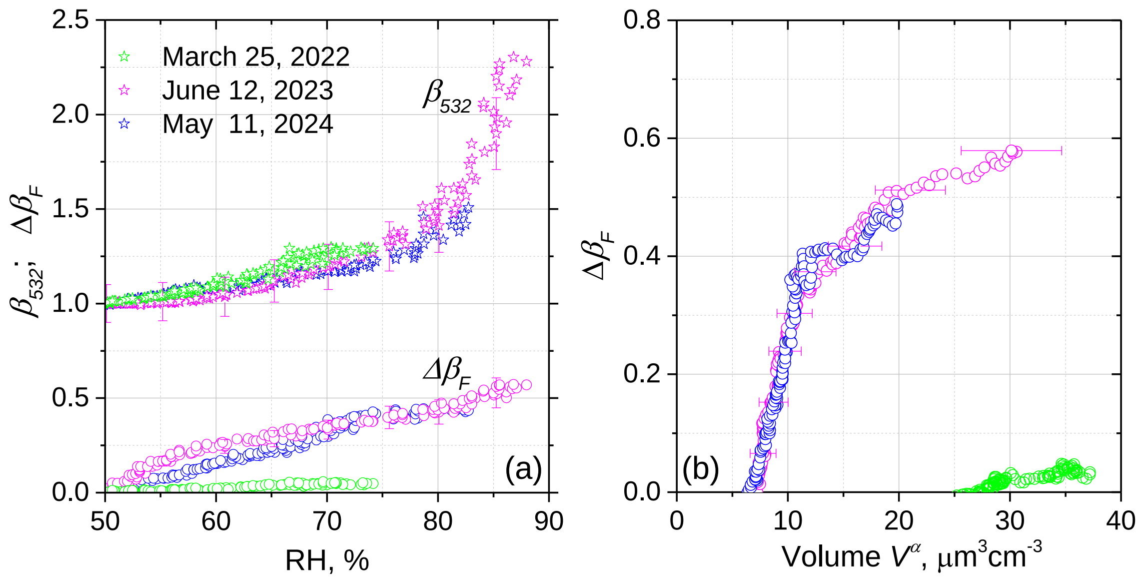

Figure 9: (a) The RH-dependence of normalized backscattering coefficient, β_{532} (stars), and fluorescence reduction, $\Delta\beta_F$ (circles), for three case studies: March 25, 2022, June 12, 2023 and May 11, 2024. All values are normalized relative to RH=50% baseline conditions. (b) The relationship between fluorescence reduction $\Delta\beta_F$ and particle volume V^{α}, calculated from α_{532}, for the same three episodes.

5 Conversion factors for smoke and urban particles

As demonstrated in the previous section, the volume density of urban aerosol, even in the presence of hygroscopic growth, can be estimated using a single extinction or backscattering coefficient, and corresponding conversion factors. However, urban aerosol includes a variety of particle types (e.g. sulfates, soot), causing these conversion factors to vary across episodes. To quantify this variability and assess the resulting uncertainty in V and S calculations, we analyzed multiple episodes of urban aerosol within the PBL exhibiting hygroscopic growth. For each episode, conversion factors at 355 nm and 532 nm were derived from $3\beta+2\alpha$ observations.

https://doi.org/10.5194/egusphere-2025-2107
Preprint. Discussion started: 15 May 2025

In addition to urban aerosols, we also examined smoke episodes. For smoke, hygroscopic growth events were rare, and our
310 focus shifted to the vertical dependence of conversion factors in the lower and middle troposphere. Fig.10 presents the vertical profiles of the conversion factors $C^V_{\alpha,532}$ and $C^V_{\beta,532}$ for ten urban aerosol episodes involving hygroscopic growth, along with six smoke episodes observed between 2021 and 2024.

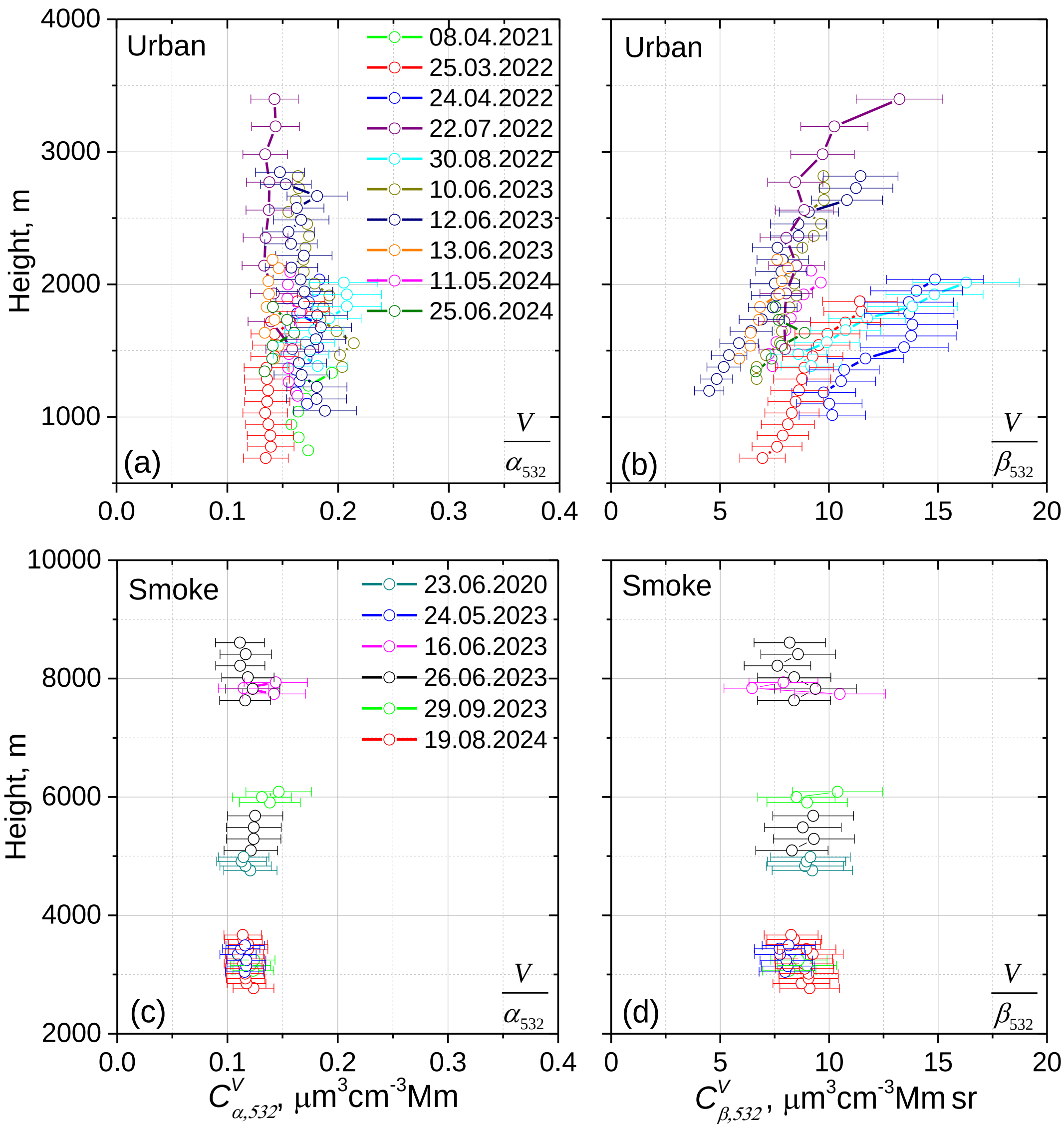

315 **Figure 10: Height profiles of the extinction-to-volume, C_V^α, and backscattering-to-volume, C_V^β, conversion factors in several measurement sessions for (a, b) urban aerosol and (c, d) smoke.**

https://doi.org/10.5194/egusphere-2025-2107
Preprint. Discussion started: 15 May 2025

For urban aerosol, the mean value of $C^{V}_{\alpha,532}$ is estimated to be 0.17±0.04 μm³cm⁻³Mm. Thus, the uncertainty of volume density estimation remains below 25%, even in the presence of hygroscopic growth. This contrasts with the higher value of 0.30 ±0.08 μm³cm⁻³Mm reported by Mamouri and Ansmann (2017) for continental aerosol in Germany. However, as previously noted, aerosol composition within the PBL can exhibit significant regional variability, likely explaining this discrepancy. In contrast to the extinction coefficient, the backscattering coefficient exhibits greater sensitivity to changes in the refractive index, leading to significantly stronger variations $C^{V}_{\beta,532}$ compared to $C^{V}_{\alpha,532}$ (Fig.10b). The mean value of $C^{V}_{\beta,532}$ is 10±6 μm³cm⁻³Mmsr, corresponding to an unacceptably high uncertainty in volume estimation (up to 60%). Consequently, for urban aerosols, reliable volume density retrievals should be based solely on the extinction coefficient.

For smoke, the mean conversion factor $C^{V}_{\alpha,532}$ is 0.13±0.02 μm³cm⁻³Mm across all height ranges, which is very close to the value of 0.13±0.08 μm³cm⁻³Mm reported by Ansmann et al. (2021) for aged smoke in AERONET measurements. The composition of smoke is less variable compared to urban aerosol, allowing for reliable volume estimations even based on the backscattering coefficient (Fig.11d). The mean value of $C^{V}_{\beta,532}$ for smoke is 9±1.5 μm³cm⁻³Mmsr, indicating comparable uncertainties in volume estimation from both extinction and backscattering coefficients for the analyzed episodes.

Table 1. Conversion factors for calculation of volume and surface of smoke and urban particles from the extinction and backscattering coefficients at 355 and 532 nm wavelengths.

	$C^{V}_{\alpha,355}$	$C^{V}_{\alpha,532}$	$C^{V}_{\beta,355}$	$C^{V}_{\beta,532}$	$C^{S}_{\alpha,355}$	$C^{S}_{\alpha,532}$	$C^{S}_{\beta,355}$	$C^{S}_{\beta,532}$
	μm³cm⁻³Mm		μm³cm⁻³Mm sr		μm²cm⁻³Mm		μm²cm⁻³Mm sr	
Urban	0.08±0.03	0.17±0.04	-	-	1.6±0.3	2.9±0.7	-	-
Smoke	0.085±0.015	0.13±0.025	4.25±1.20	9±2.0	1.3±0.25	1.75±0.4	60±20	125±50

Table 1 summarizes the conversion factors for calculating particle volume and surface density for the episodes presented in Fig.10. The conversion factors $C^{V}_{\beta,\lambda}$ and $C^{S}_{\beta,\lambda}$ for urban aerosol are excluded, due to their unacceptably high uncertainties. For aged smoke, we obtain $C^{S}_{\alpha,532}$ =1.75±0.4 μm²cm⁻³Mm, which agrees well with the value 1.75±0.25 μm²cm⁻³Mm reported by Ansmann et al. (2021). These findings demonstrate that in numerous cases, both particle volume and surface density of smoke can be retrieved from either a single extinction or backscattering coefficient, which is - particularly valuable when complete 3β+2α measurements are unavailable.

Conclusion

https://doi.org/10.5194/egusphere-2025-2107
Preprint. Discussion started: 15 May 2025

We analyzed Mie-Raman-Fluorescence lidar observations during aerosol hygroscopic growth episodes to investigate water uptake effects on fluorescence backscattering, β_F. The well-mixed PBL serves as a convenient environment for such studies, since β_F should remain constant in the absence of water uptake effects. However, during certain episodes we observed a systematic height-dependent decrease in β_F. This observed β_F reduction is difficult to explain solely by changes in aerosol composition and likely indicates fluorescence quenching. Notably, the decrease in β_F begins at relatively low RH (less than 50%), coinciding with a reduction in the depolarization ratio. Interestingly, while β_{532} shows rapid enhancement at high RH levels, this is not accompanied by an accelerated β_F decrease rate.

Our observations demonstrate that fluorescence quenching exhibits strong dependence on aerosol composition, as evidenced by its absence in numerous episodes. While we cannot yet identify the specific particle type responsible for this quenching effect, we confirm that the process does not alter the fluorescence spectral signature. When fluorescence measurements are made using multiple discrete channels, the ratio of fluorescence backscattering coefficients between these channels remains unaffected by water uptake, although each individual channel is influenced by it (see Fig.10 in Veselovskii et al., 2025).

The particle volume and surface density, retrieved from $3\beta+2\alpha$ measurements during analysis of hygroscopic growth episodes were used to validate the feasibility of estimating these parameters from a single extinction coefficient. Our analysis shows that for urban aerosols, the uncertainty in V and S determination remains below 25% when using α_{532}. Smoke particles demonstrate comparable uncertainties in V and S calculation. The conversion factors show clear dependence on aerosol type, which can be effectively identified through fluorescence lidar measurements. These findings highlight the Mie-Raman-Fluorescence lidar as a promising tool for aerosol characterization.

Data availability. Lidar measurements are available upon request (philippe.goloub@univ-lille.fr).

Author contributions. IV processed the data and wrote the paper. QH performed meteorological analysis. TP and GD performed lidar measurements. PG supervised the project and helped with paper preparation. AK performed numerical simulations and MK developed the software for data analysis.

.

Competing interests. The authors declare that they have no conflict of interests.

Acknowledgement

We acknowledge funding from the CaPPA project funded by the ANR through the PIA under contract ANR-11-LABX-0005-01, the “Hauts de France” Regional Council (project ECRIN) and the European Regional Development Fund (FEDER). ESA/QA4EO program is greatly acknowledged for supporting the observation activity at LOA. The work of Q. Hu was supported by Agence Nationale de Recherhce ANR (ANR-21-ESRE-0013) through the OBS4CLIM project. The Russian Science Foundation is acknowledged for its supports in the framework of project 21-17-00114. This work has benefited from the supports of the research infrastructure ACTRIS-FR, registered on the Roadmap of the French Ministry of Research » as well as from the Center of Aerosol Remote Sensing (CARS) of the ACTRIS-EU research infrastructure

https://doi.org/10.5194/egusphere-2025-2107
Preprint. Discussion started: 15 May 2025

References

Ansmann, A., Ohneiser, K., Mamouri, R.-E., Knopf, D. A., Veselovskii, I., Baars, H., Engelmann, R., Foth, A., Jimenez, C., Seifert, P., and Barja, B.: Tropospheric and stratospheric wildfire smoke profiling with lidar: Mass, surface area, CCN and INP retrieval, Atmos. Chem. Phys., 21, 9779–9807, https://doi.org/10.5194/acp-21-9779-2021, 2021.

Burton, S. P., Ferrare, R. A., Hostetler, C. A., Hair, J.W., Rogers, R. R., Obland, M. D., Butler, C. F., Cook, A. L., Harper, D. B., and Froyd, K. D.: Aerosol classification using airborne High Spectral Resolution Lidar measurements – methodology and examples, Atmos. Meas. Tech., 5, 73–98, https://doi.org/10.5194/amt-5-73-2012, 2012.

Carrico, C. M., Kus, P., Rood, M. J., Quinn, P. K., and Bates, T. S.: Mixtures of pollution, dust, sea salt, and volcanic aerosol during ACE-Asia: Radiative properties as a function of relative humidity, J. Geophys. Res., 108, 8650, https://doi.org/10.1029/2003JD003405, 2003.

Chang, Y.; Hu, Q.; Goloub, P.; Veselovskii, I.; Podvin, T.: Retrieval of Aerosol Microphysical Properties from Multi-Wavelength Mie–Raman Lidar Using Maximum Likelihood Estimation: Algorithm, Performance, and Application. Remote. Sens. 14, 6208, https://doi.org/10.3390/rs14246208, 2022.

Chen, J., Li, Z., Lv, M., Wang, Y., Wang, W., Zhang, Y., Wang, H., Yan, X., Sun, Y., and Cribb, M.: Aerosol hygroscopic growth, contributing factors, and impact on haze events in a severely polluted region in northern China, Atmos. Chem. Phys., 19, 1327–1342, https://doi.org/10.5194/acp-19-1327-2019, 2019.

Chin, M., Ginoux, P., Kinne, S., Torres, O., Holben, B., Duncan, B., Martin, R.V., Logan, J.A., Higurashi, A., Nakajima, T.: Tropospheric aerosol optical thickness from the GOCART model and comparisons with satellite and Sun photometer measurements, Journal of the Atmospheric Sciences, 59, 461–483, 2002.

Colarco, P., Da Silva, A., Chin, M., and Diehl, T.: Online simulations of global aerosol distributions in the NASA GEOS-4 model and comparisons to satellite and ground-based aerosol optical depth. Journal of Geophysical Research 115, doi.10.1029/2009JD012820, 2010.

Dawson, K. W., Ferrare, R. A., Moore, R. H., Clayton, M. B., Thorsen, T. J., and Eloranta, E. W.: Ambient Aerosol Hygroscopic Growth From Combined Raman Lidar and HSRL, J. Geophys. Res.-Atmos., 125, e2019JD031708, https://doi.org/10.1029/2019JD031708, 2020.

Dobretsov, G.E., Syrejschikova, T.I. and Smolina, N.V.: On mechanisms of fluorescence quenching by water. Biophysics 59, 183–188, https://doi.org/10.1134/S0006350914020079, 2014.

Feingold, G. and Morley, B.: Aerosol hygroscopic properties as measured by lidar and comparison with in situ measurements, J. Geophys. Res., 108, 4327, https://doi.org/10.1029/2002JD002842, 2003.

Fernández, A. J., Apituley, A., Veselovskii, I., Suvorina, A., Henzing, J., Pujadas, M., and Artíñano, B.: Study of aerosol hygroscopic events over the Cabauw experimental site for atmospheric research (CESAR) using the multiwavelength Raman lidar Caeli, Atmos. Environ., 120, 484–498, https://doi.org/10.1016/j.atmosenv.2015.08.079, 2015.

Floutsi, A. A., Baars, H., Engelmann, R., Althausen, D., Ansmann, A., Bohlmann, S., Heese, B., Hofer, J., Kanitz, T., Haarig, M., Ohneiser, K., Radenz, M., Seifert, P., Skupin, A., Yin, Z., Abdullaev, S. F., Komppula, M., Filioglou, M., Giannakaki, E., Stachlewska, I. S., Janicka, L., Bortoli, D., Marinou, E., Amiridis, V., Gialitaki, A., Mamouri, R.-E., Barja, B., and Wandinger, U.: DeLiAn – a growing collection of depolarization ratio, lidar ratio and Ångström exponent for different aerosol types and mixtures from ground-based lidar observations, Atmos. Meas. Tech., 16, 2353–2379, https://doi.org/10.5194/amt-16-2353-2023, 2023.

Gast, B., Jimenez, C., Ansmann, A., Haarig, M., Engelmann, R., Fritzsch, F., Floutsi, A. A., Griesche, H., Ohneiser, K., Hofer, J., Radenz, M., Baars, H., Seifert, P., and Wandinger, U.: Invisible aerosol layers: improved lidar detection capabilities by means of laser-induced aerosol fluorescence, EGUsphere [preprint], https://doi.org/10.5194/egusphere-2024-2586, 2024.

Granados-Muñoz, M. J., Navas-Guzmán, F., Bravo-Aranda, J. A., Guerrero-Rascado, J. L., Lyamani, H., Valenzuela, A., Titos, G., Fernández-Gálvez, J., and Alados-Arboledas, L.: Hygroscopic growth of atmospheric aerosol particles based on active remote sensing and radiosounding measurements: selected cases in southeastern Spain, Atmos. Meas. Tech., 8, 705–718, https://doi.org/10.5194/amt-8-705-2015, 2015.

Haarig, M., Ansmann, A., Gasteiger, J., Kandler, K., Althausen, D., Baars, H., Radenz, M., and Farrell, D. A.: Dry versus wet marine particle optical properties: RH dependence of depolarization ratio, backscatter, and extinction from multiwavelength lidar measurements during SALTRACE, Atmos. Chem. Phys., 17, 14199–14217, https://doi.org/10.5194/acp-17-14199-2017, 2017.

Haarig, M., Engelmann, R., Baars, H., Gast, B., Althausen, D., and Ansmann, A.: Discussion of the spectral slope of the lidar ratio between 355 nm and 1064 nm from multiwavelength Raman lidar observations, EGUsphere [preprint], https://doi.org/10.5194/egusphere-2025-449, 2025.

Hänel, G.: The Properties of Atmospheric Aerosol Particles as Functions of the Relative Humidity at Thermodynamic Equilibrium with the Surrounding Moist Air, Adv. Geophys., 19, 73–188, 1976.

He, Y., Yin, Z., Ansmann, A., Liu, F., Wang, L., Jing, D., and Shen, H.: POLIPHON conversion factors for retrieving dust-related cloud condensation nuclei and ice-nucleating particle concentration profiles at oceanic sites, Atmos. Meas. Tech., 16, 1951–1970, https://doi.org/10.5194/amt-16-1951-2023, 2023.

Kolgotin, A., Müller, D., Chemyakin, E., Romanov, A., and Alehnovich, V.: Improved identification of the solution space of aerosol microphysical properties derived from the inversion of profiles of lidar optical data, part 3: case studies, Appl. Opt., Vol. 57, 2499-2513, 2018.

Kolgotin, A., Müller, D., and Romanov, A.: Particle microphysical parameters and the complex refractive index from 3β + 2α HSRL/Raman lidar measurements: conditions of accurate retrieval, retrieval uncertainties and constraints to suppress the uncertainties, Atmosphere 2023, 14, 1159. https://doi.org/10.3390/atmos14071159.

Kolgotin, A., Muller, D., Goloub, P., Hu, Q., Podvin, T., and Wang, X.: Aerosol Typing from Linear estimations for the Analytical Separation (ATLAS) of complex aerosol mixtures and improved identification of microphysical parameters from multiwavelength lidar data, part 2: case studies, JOSA A, Vol. 42, 233-253, https://doi.org/10.1364/JOSAA.537287, 2025.

Maillard, J., Klehs, K., Rumble, C., Vauthey, E., Heilemann, M., Fürstenberg, A.: Universal quenching of common fluorescent probes by water and alcohols, Chem. Sci.,12, 1352-1362, https://doi.org/10.1039/d0sc05431c, 2021.

Mamouri, R.-E., and Ansmann, A.: Potential of polarization/Raman lidar to separate fine dust, coarse dust, maritime, and anthropogenic aerosol profiles, Atmos. Meas. Tech., 10, 3403–3427, https://doi.org/10.5194/amt-10-3403-2017, 2017.

Miri, R., Pujol, O., Hu, Q., Goloub, P., Veselovskii, I., Podvin, T., and Ducos, F.: Innovative aerosol hygroscopic growth study from Mie–Raman–fluorescence lidar and microwave radiometer synergy, Atmos. Meas. Tech., 17, 3367–3375, https://doi.org/10.5194/amt-17-3367-2024, 2024.

Navas-Guzmán, F., Martucci, G., Collaud Coen, M., Granados-Muñoz, M. J., Hervo, M., Sicard, M., and Haefele, A.: Characterization of aerosol hygroscopicity using Raman lidar measurements at the EARLINET station of Payerne, Atmos. Chem. Phys., 19, 11651–11668, https://doi.org/10.5194/acp-19-11651-2019, 2019.

Pérez-Ramírez, D., Whiteman, D. N., Veselovskii, I., Ferrare, R., Titos, G., Granados-Muñoz, M. J., Sánchez-Hernández, G., and Navas-Guzmán, F.: Spatiotemporal changes in aerosol properties by hygroscopic growth and impacts on radiative forcing and heating rates during DISCOVER-AQ 2011, Atmos. Chem.Phys., 21, 12021–12048, https://doi.org/10.5194/acp-21-12021-2021, 2021.

Randriamiarisoa, H., Chazette, P., Couvert, P., Sanak, J., and Mégie, G.: Relative humidity impact on aerosol parameters in a Paris suburban area, Atmos. Chem. Phys., 6, 1389–1407, https://doi.org/10.5194/acp-6-1389-2006, 2006.

Raut, J.-C. and Chazette, P.: Vertical profiles of urban aerosol complex refractive index in the frame of ESQUIF airborne measurements, Atmos. Chem. Phys., 8, 901–919, https://doi.org/10.5194/acp-8-901-2008, 2008.

Reichardt, J., Lauermann, F., and Behrendt, O.: Fluorescence spectra of atmospheric aerosols, EGUsphere [preprint], https://doi.org/10.5194/egusphere-2024-3928, 2024.

Sheridan, P. J., Delene, D. J., and Ogren, J. A.: Four years of continuous surface aerosol measurements from the Department of Energy's Atmospheric Radiation Measurement Program Southern Great Plains Cloud and Radiation Testbed site, J. Geophys. Res., 106, 20735–20747, https://doi.org/10.1029/2001JD000785, 2001.

Sicard, M., Fortunato dos Santos Oliveira, D. C., Muñoz-Porcar, C., Gil-Díaz, C., Comerón, A., Rodríguez-Gómez, A., and Dios Otín, F.: Measurement report: Spectral and statistical analysis of aerosol hygroscopic growth from multi-wavelength lidar measurements in Barcelona, Spain, Atmos. Chem. Phys., 22, 7681–7697, https://doi.org/10.5194/acp-22-7681-2022, 2022.

Veselovskii I., Kolgotin, A., Griaznov, V., Müller, D., Wandinger, U., Whiteman, D.: Inversion with regularization for the retrieval of tropospheric aerosol parameters from multi-wavelength lidar sounding, Appl.Opt. 41, 3685-3699, https://doi.org/10.1364/AO.41.003685, 2002.

Veselovskii, I., Whiteman, D. N., Kolgotin, A., Andrews, E., and Korenskii, M.: Demonstration of Aerosol Property Profiling by Multiwavelength Lidar under Varying Relative Humidity Conditions, J. Atmos. Ocean. Tech., 26, 1543–1557, https://doi.org/10.1175/2009JTECHA1254.1, 2009.

Veselovskii, I., Hu, Q., Goloub, P., Podvin, T., Korenskiy, M., Pujol, O., Dubovik, O., Lopatin, A.: Combined use of Mie-Raman and fluorescence lidar observations for improving aerosol characterization: feasibility experiment, Atm. Meas. Tech., 13, 6691–6701, doi.org/10.5194/amt-13-6691-2020, 2020.

Veselovskii, I., Barchunov, B., Hu, Q., Goloub, P., Podvin, T., Korenskii, M., Dubois, G., Boissiere, W., and Kasianik, N.: Retrieval and analysis of the composition of an aerosol mixture through Mie–Raman–fluorescence lidar observations, Atmos. Meas. Tech., 17, 4137–4152, https://doi.org/10.5194/amt-17-4137-2024, 2024.

Veselovskii, I., Korenskiy, M., Kasianik, N., Barchunov, B., Hu, Q., Goloub, P., and Podvin, T.: Fluorescence properties of long-range-transported smoke: insights from five-channel lidar observations over Moscow during the 2023 wildfire season, Atmos. Chem. Phys., 25, 1603–1615, https://doi.org/10.5194/acp-25-1603-2025, 2025.

Zhou, Z.; Ma, Y.; Yin, Z.; Hu, Q.; Veselovskii, I.; Müller, D.; Gong, W. A Modified Look-Up Table Based Algorithm with a Self-Posed Scheme for Fine-Mode Aerosol Microphysical Properties Inversion by Multi-Wavelength Lidar. Remote Sens., 16, 2265. https://doi.org/10.3390/rs16132265, 2024.